Structures 51 (2023) 970–984

Contents lists available at ScienceDirect

Structures

journal homepage: www.elsevier.com/locate/structures

Design, construction and performance of the Monash pultruded glass fibre-reinforced polymer footbridge

Colin C. Caprani [a,*], Jun Wei Ngan [a], Ehsan Ahmadi [a,b], Shao Hua Zhang [a], Yu Bai [a], Sindu Satasivam [a]

[a] Department of Civil Engineering, Monash University, Melbourne, Australia
[b] Department of Civil Engineering, Birmingham City University, United Kingdom

ARTICLE INFO

Keywords:
Pultruded glass fibre-reinforced polymer
Sandwich panel
Footbridge
Design
Construction process
Finite element
Static performance
Vibration serviceability performance

ABSTRACT

This paper describes the design, construction, and performance testing of the Monash Bridge (MB). The MB is a pultruded glass fibre-reinforced (pGFRP) footbridge built from individual standard pGFRP sections bonded using epoxy. The MB is designed to conform to current guidelines for GFRP footbridges in order to evaluate their performance. The design process of the MB is facilitated with numerical modelling techniques. This paper details the construction method of the MB, from which lessons that are learned may be relevant to other similar constructions. The construction process shows the potential of epoxy-bonding in practical construction of similar structures. This paper also reports on the performance of the MB, namely the static and dynamic performances. While the static performance is shown to be good, testing showed high levels of acceleration responses during walking trials, indicating that current vibration rules are not generally applicable for GFRP footbridges and that more advanced assessment of vibration serviceability should be conducted for new designs.

1. Introduction

1.1. Background

In the last few decades, glass fibre-reinforced polymer (GFRP) composites have been increasingly applied in footbridge construction. This stems from the mechanical and structural advantages of GFRP composites: its light weight yields benefits such as rapid construction, minimal disruption as well as low labour costs [1]; while its excellent durability and corrosion resistance permits lower maintenance cost, making it particularly well-suited for the replacement of deteriorated footbridges [2]. Indeed, the application of GFRP footbridges is also motivated by the pressing need to replace deteriorating bridges with more durable materials [3]. However, there is still reluctance for using GFRP in bridge construction due to a lack of structural performance data [4,5]. For bridge structural forms, the application of GFRP composites can either be hybrid (combining with conventional steel or concrete forms) or fully constructed from GFRP. The scope of this paper focuses on latter of the applications of GFRP.

Pultruded GFRP (pGFRP) is a means of manufacturing regular structural section shapes from GFRP. It is an efficient manufacturing process and facilitates much cheaper production and hence construction than laid-up laminated GFRP. Besides the chopped strand mat surface veils in pGFRP, the main structural fibres are oriented in one direction (longitudinal), which makes pGFRP an orthotropic material, and so more prone to cracking in the other direction (transverse) when subjected to loading [6]. In addition, the limit state design of load-carrying structural members using pGFRP is often decided by those of serviceability (e.g., deflection and vibration). This stems from the relatively low elastic modulus of pGFRP (approximately 12% of steel [7]). A common way to compensate for the low elastic modulus is to consider structural forms such as truss or sandwich construction which increase the flexural rigidity.

To ensure a high stiffness in the longitudinal and transverse directions, a novel, orthotropic pGFRP sandwich assembly was proposed [6] —see Fig. 1. The modular sandwich panel comprises pGFRP box profiles incorporated between pGFRP flat panels. A bidirectional fibre orientation was adopted in the sandwich panel system – the pultrusion direction of box profile layer is perpendicular to the flat sheet layer – giving optimized strength in both orthogonal directions. The benefits of lightweight, strong, and durable footbridges are achievable when adopting the pGFRP sandwich system for the superstructure of a

* Corresponding author.
E-mail address: colin.caprani@monash.edu (C.C. Caprani).

https://doi.org/10.1016/j.istruc.2023.03.090
Received 18 November 2022; Received in revised form 17 March 2023; Accepted 17 March 2023
Available online 27 March 2023

footbridge. In addition, the modular construction method is beneficial for bridge applications in terms of quality and control as well as offering quick on-site assembly. To date, the mechanical properties of this sandwich panel have been investigated by constructing and testing scaled-down specimens including sandwich beams [8,9], two-way spanning slabs [10], and pGFRP-steel composite beams [11]. These studies have demonstrated the competitive potential of the proposed sandwich panel as structural members.

1.2. Contributions

The concept of full-pGFRP construction for footbridges has been adopted in many as-built footbridges around the world [12]. For example, the first reported FRP Bridge was in Miyun, Beijing in 1982 [13]. In the United States, No-Name Creek Bridge is the first all-FRP honeycomb core sandwich panel bridge [14]. Currently, the Alberfeldy Bridge in Scotland is the world's longest GFRP cable-stayed footbridge – with a main span of 63 m [15]. Notably, the majority of pGFRP footbridges were manufactured by either constructing customized sections or modular construction - connecting proprietary GFRP sections [12,16]. However, it appears that a limited number of pGFRP footbridges adopted the combination of: (1) modular construction, and (2) adhesive bonding connections. The closest examples (the Leri and Dawlish footbridges) utilize an adhesively-bonded deck combined with steel bolts in several locations [16]. Consequently, the application of the proposed pGFRP sandwich panel in footbridges along with these two aspects can enhance the range of potential GFRP footbridge designs.

One of the obstacles for the widespread application of GFRP composites in civil engineering is the lack of internationally accepted design standards. In particular, there only four guides for GFRP footbridges (i.e., [17–20]) and even those often use design approaches developed for traditional steel and concrete structures [21]. As a pertinent example, the AASHTO GFRP Bridge Design Guide [19] and Highways England CD 368 [20] specify the 5 Hz 'rule-of-thumb' in which vibration problems are deemed unlikely as long as the fundamental natural frequency of GFRP footbridges is at least 5 Hz. This rule-of-thumb assumes that the higher harmonics of human-induced forces will not cause vibration problems. However, this threshold frequency was determined as adequate in the past from experience with much heavier concrete and steel footbridges. But with the different properties of GFRP composites—the strength of steel, stiffness of concrete, and weight of dense timber—the solutions from these design rules may not be appropriate for GFRP footbridges. Specifically, and as will be shown later, GFRP structures have a higher accelerance (acceleration per unit harmonic force) [22,23], making them potentially more susceptible to human-induced vibrations. Therefore, comprehensive performance testing of GFRP footbridge variations will enable evaluation of design rules and fully-explore the merits of GFRP composites in bridge construction.

To explore the gaps in current practice, a pGFRP footbridge comprised of: (1) the proposed orthotropic sandwich deck in Fig. 1; (2) a modular construction method, and (3) adhesive bonding for connections, is designed in accordance with current guidelines. In regards to performance testing, most published works have covered static performance [24] and dynamic performance of existing GFRP footbridges [15,25–28]. However, as most of the published work on GFRP footbridges relates to laminated GFRP [29,30], knowledge of structural design and performance of pGFRP footbridges remains limited [23,31,32]. Thus, this work aims to further contribute to:

(1) Relevant manufacturing issues of modular, epoxy-bonded pGFRP sandwich structures.
(2) The static and dynamic performance of a full-scale orthotropic sandwich deck epoxy-bonded pGFRP footbridges.

This paper presents a full-scale orthotropic sandwich deck epoxy-bonded pGFRP footbridge which has been constructed and tested at Monash University – denoted as the Monash Bridge (MB). The MB's design process based on numerical modelling techniques as well as design checks to guidelines for GFRP footbridge are briefly presented. Subsequently, the construction concept and processes are described. In addition, the evaluation of structural performance based on data of comprehensive experimental testing of the MB are presented in this paper.

2. Design

2.1. Overview of the MB

The MB is a 9 m long, twin girder footbridge as illustrated in Fig. 2. The deck of the MB comprises the modular pGFRP sandwich panel, made from individual pGFRP box profiles and flat panels, which spans transversely between two pGFRP I-beam girders that are in turn supported at both ends. As described previously, the fibres directions of pGFRP sections are aligned in a bidirectional orientation to increase overall stiffness in orthogonal directions - preventing cracking in the weaker transverse (box fibre) direction. All structural connections of the MB use epoxy bonding. The MB has a mass per unit length of 92.56 kg/m, making it a very lightweight footbridge. A comparable steel–concrete laboratory footbridge—the Warwick University footbridge [33]—has a linear mass of 829 kg/m [34]. To reduce extraneous sources of uncertainties in design and analysis, the MB was built with no external attachments, such as handrails for example. The bridge span can be altered by moving the underlying supports.

2.2. Research-driven design requirements

In addition to its conducive structural form, the MB was purpose-designed for multiple study objectives, including:

- **Study 1**: Feasibility and manufacture of all-epoxy bonding and modular construction for pGFRP structures.

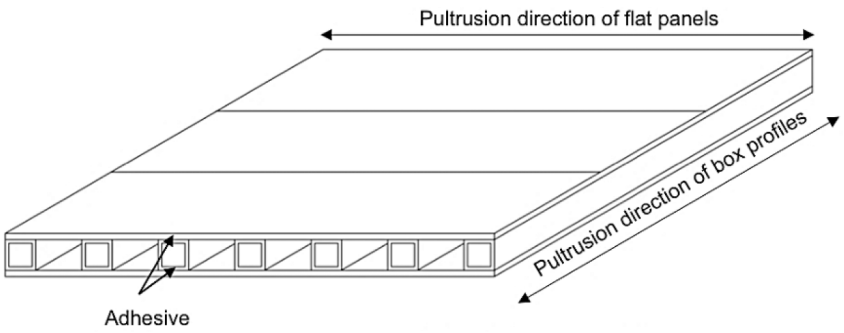

Fig. 1. pGFRP sandwich panel system, showing fibre directions of components (after [10]).

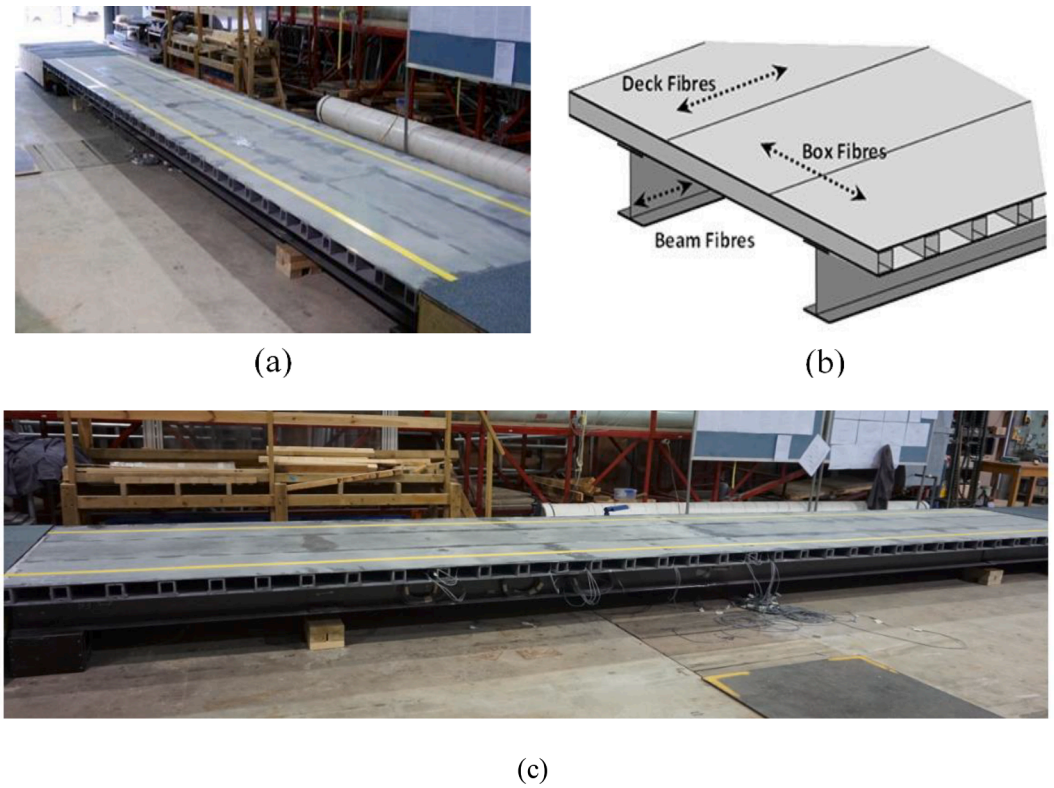

Fig. 2. Overview of the MB: (a) photograph view; (b) composite section showing fibre orientations of different components; (c) side view.

- **Study 2**: Evaluation of human-structure interactions (HSI) in lightweight and lightly-damped structures.
- **Study 3**: Evaluation of design rules for pGFRP footbridges.

An experimental footbridge realized with pGFRP composites fulfils the requirement for Study 1 and 2. Considerations of both epoxy bonding and modular construction of standard sections (e.g., box profiles and flat sheets) in the manufacturing process of the MB fulfils the

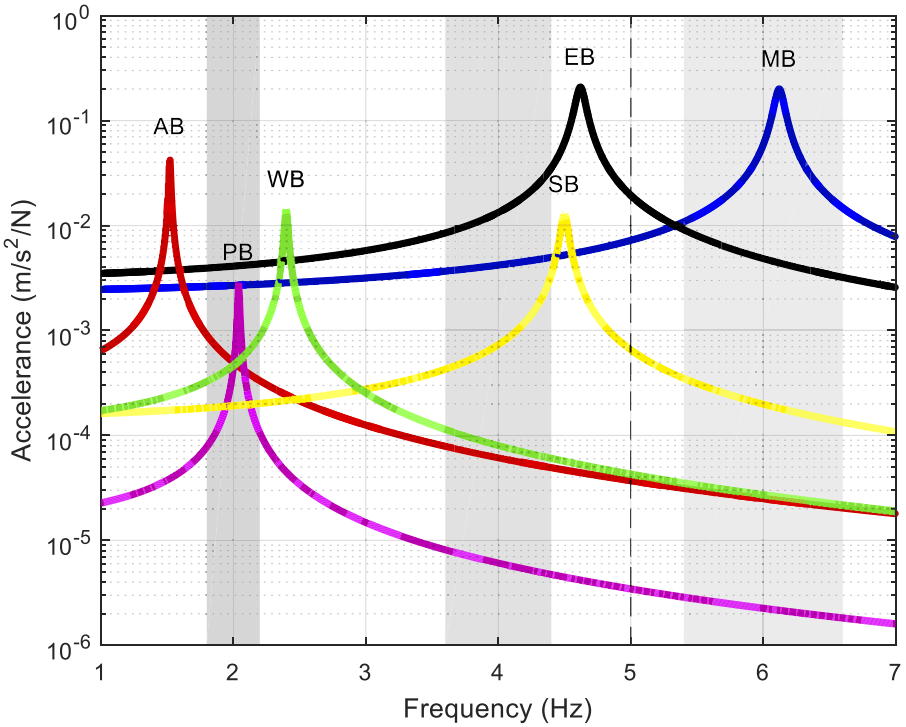

Fig. 3. Relationship of first mode FRFs (accelerance) between different footbridges; typical walking harmonics (shaded grey), and the 5 Hz rule (dashed line). AB – Aberfeldy Footbridge (GFRP); PB – Podgoricia Bridge (Steel); WB – Warwick Bridge (Steel-Concrete Composite); SB – Sheffield Bridge (Concrete); EB – EMPA Bridge (GFRP deck); MB – Monash Bridge (pGFRP) (data from [23]).

requirement of Study 1. The relatively lower mass and damping of pGFRP composites compared to typical concrete and steel infers an overall lightweight and lightly-damped bridge structure, making the MB a suitable benchmark structure for Study 2.

The requirement for Study 3 is achieved by designing the dynamic behaviour of the MB. In terms of accelerance (acceleration per unit force), the targeted dynamic behaviour of the MB, compared with several comparable footbridges reported in Živanović [23] is shown in Fig. 3. The harmonic ranges of common walking frequencies (e.g. first harmonic from 1.8 Hz to 2.2 Hz [35]) have been shaded, and the common 5 Hz rule is shown as a dashed line in Fig. 3. It is commonly assumed that excitations of higher harmonics (more than two) are negligible when applying the 5 Hz rule. Therefore, the performance of the 5 Hz rule can be assessed by checking the vibrations levels of the MB from higher walking harmonics – fulfilling scope of Study 2. To do this, the MB is designed with a first natural frequency, f_1 within the third harmonic range of walking frequencies (between 5.4 Hz and 6.6 Hz).

2.3. Material characterization

As the design checks precede the construction of the MB, it is important that the FE model results are accurate. To improve the fidelity of the numerical results, the material properties of pGFRP in the FE model were obtained through comprehensive tensile testing of pGFRP coupons cut from sacrificial sheets and members corresponding to various components of the footbridge [36]. The coupons were taken for two thicknesses – 6 mm (flat panel, connecting plates, and I-beams) and 9 mm (box profiles). For each thickness, ten specimens were longitudinal and transverse to the fibre pultrusion direction. The tests were performed using the 100 kN Instron Universal Testing Machine in accordance to ASTM 3039 [37]. In addition, 6 mm-thick pGFRP coupons of size 250 × 25 mm were extracted on a 10° off-axis angle cut and tested (similar to [38]) to determine the in-plane shear modulus, G_{LT}. Preliminary burn-off tests shows the fibre volume fraction (FVF) of the pGFRP components is 42.1 ± 0.3% [36].

Table 2 summarizes the material properties of pGFRP which are comprised of the longitudinal and transverse elastic modulus in tension, longitudinal tensile strength, and the in-plane shear modulus. These properties were taken from averages of the ten specimens. The coefficients of variation (CoV) are also summarized in Table 2 for the 6 mm thickness. The elastic moduli and Poisson's ratios for both thicknesses were found using Hooke's law [36]. As can be seen, the material properties are very similar between the two coupon thicknesses. As a result, it is reasonable to assume the differences in material properties are negligible between 9 mm and 6 mm coupons. Therefore, the material properties for the 6 mm coupons are considered for all components within the FE model since it encompasses in-plane shear modulus.

2.4. Design process and outcomes

Numerical modelling is adopted for the design of the MB. Specifically, a finite element (FE) model of the MB is developed in LUSAS software [39] to predict the structural behavior for design checks. The numerical predictions from the FE model are later compared with experimental measurements of static (deflections and strain) and dynamic (mode shapes and natural frequencies) performances.

The FE model of the MB is shown in Fig. 4. All structural components, including flat panels, box sections, and bottom I-beam girders were modelled using eight-node quadrilateral shell elements (QTS8). This shell element has six degrees of freedom at each node: translation in nodal x ,y, and z directions and rotation about nodal x ,y, and z axes. All regions with multiple connected pGFRP components (e.g., between beam flange and flat panel) were modelled as an equivalent shell element with combined thickness of connected components. The orthotropic properties of pGFRP were defined for the shell elements considering the fibre directions of components according to Fig. 2b. The bonds or interfaces between components (e.g., between bottom deck panel and I-girder top flange), are not modelled. Instead, a combined thickness is assumed for the all bonded components – this is reasonable since full-composite action was observed, see [11]. Horizontal restraints were implemented at the support nodes to limit the responses (i.e., deflections and accelerations) to the vertical direction. Initially, pinned supports were considered at both ends of the I-beam girders for the design checks. For the analysis of the footbridge's dynamic behaviour,

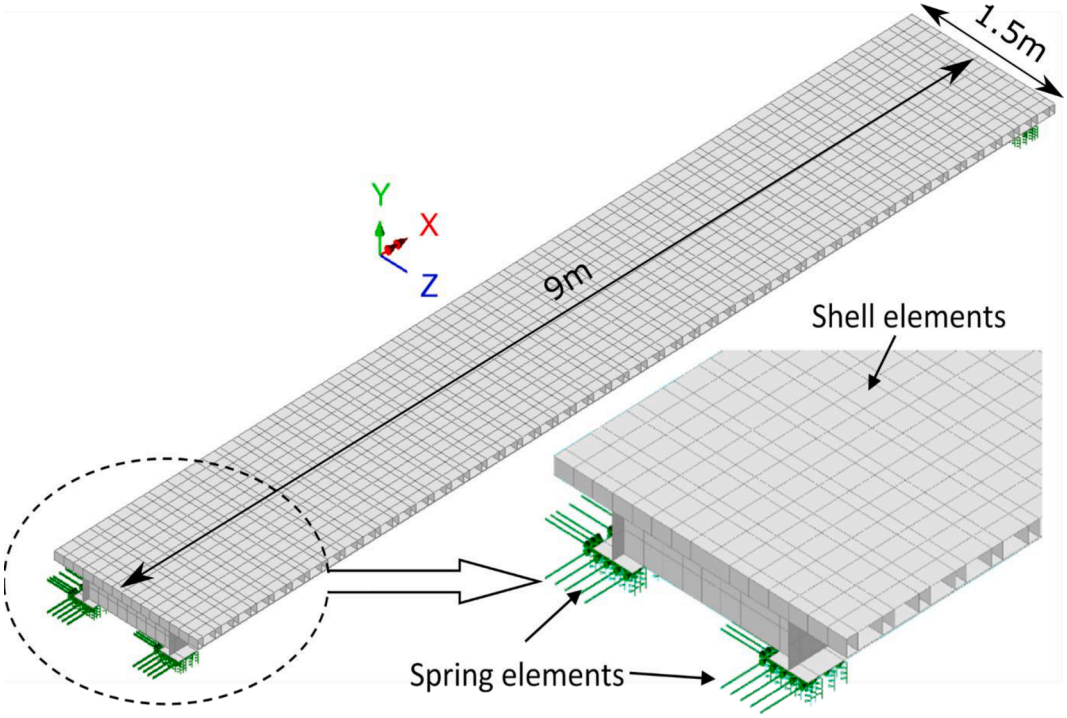

Fig. 4. The FE model of the MB used for design and comparison to experimental results.

vertical spring elements are used to represent the support flexibility in the footbridge system; the width of each spring support is approximately 107.5 mm. In turn, the span of the entire 9 m long MB is 8.785 m - considering the center-to-center distance between spring support regions.

Design for the MB comprised an allowable stress design and deflection check according to the AASHTO GFRP Bridge Design Guide [19]. A nominal uniformly-distributed load of 4.07 kN/m^2 (AASHTO's [19] requirement for serviceability) is considered as the design service load for both design checks. Two span configurations of the MB were considered in the design check: the original 8.785 m span and a shorter 6 m span. Prior to the development of the detailed FE model, an initial scheme design was developed using basic hand calculations. A static load simulation of the nominal uniformly-distributed load on the deck surface of the FE model is performed to obtain the stress and deflection responses of structural components. For the stress check, the maximum allowable stress of sections under checking must not exceed 20% (or 68 MPa) of corresponding strength capacity (which for this pGFRP is a tensile strength of 340 MPa as specified by the manufacturer, Exel Composites). The maximum deflection at midspan under the design service load is limited to 1/500 of the bridge's span, which corresponds to 12 mm and 18 mm for the 6 m and 8.785 m span configurations, respectively.

The outcomes of design checks are summarized in Table 1. As can be seen, the 6 m span of the MB conforms with the stress check. Although the deflection requirement was targeted for this span in the initial hand-calculation scheme design, it was overly stiff, and the evolved final design exceeds the deflection limit at 17.7 mm. It's worth noting that both stress and deflection requirements are met for a span of 5.62 m (deflection of 11.96 mm). Of course, the deflection limit is also exceeded for the 8.785 m span (88.8 mm). Nevertheless, the non-conformance of the deflection criteria is taken as a compromise to achieve the targeted dynamic behaviour – first natural frequency of about 6.2 Hz. Indeed, the intention of Study 2 means the first natural frequency should also remain well within the third harmonic range of walking excitation whist satisfying vibration serviceability design rule i.e., the 5 Hz requirement. Consequently, the final geometry of the MB is finalized—albeit with non-conforming deflection checks for the two spans examined in detail.

3. Construction

3.1. Modular concept

The sandwich deck of the MB adopts a modular construction scheme using individual pGFRP members. Unlike the Advanced Composites Component system [40], where pGFRP decks consist of prefabricated composite building parts, the individual pGFRP members consist of standard sections i.e. flat panels and box profiles.

Figure 5 (a-c) shows the final dimensions of the MB. The pGFRP flat panels comes in length of either 1.5 m or 3 m, and width of 0.5 m. In turn, the flat panels are connected in a staggered configuration to form the 1.5 m wide deck surface of the MB as shown in Fig. 5a. To ensure strength and stress continuity in the longitudinal direction, the flat panels are connected to adjacent panels using 6 mm-thick pGFRP connecting plates bonded from within the sandwich panel deck. Individual pGFRP box profiles with dimensions of 76 × 76 × 9.5 mm span in the transverse direction of the sandwich deck, forming the core layer. The girders consist of pGFRP I-beam with dimensions of 203 × 203 × 9 mm. The maximum available length of the individual I-beams is 6 m. In turn, two segmented I-beams (a 3 m and a 6 m length) were connected by pGFRP connecting plates along the webs and flanges to form the 9 m long I-beam.

In addition, five pGFRP T-beam sections were incorporated between the two girders to add transverse stiffness and stability against distortion. Fig. 6 shows the layout of these T-beam sections at different cross-sections along the MB. For Study 3, these stiffeners also serve to prevent unwanted localized vibrational modes pertinent to I-beams that would pollute the responses from global bending and torsional modes. The T-beams are attached to the webs of the I-beams using pGFRP equal angles and the method of connection is by adhesive bonding.

Table 1
Summary of design checks for the MB. Limits for deflection criteria are given in brackets.

Design checks	Limit	Span configuration 8.785 m	6 m
Allowable stress design	Less than 68 MPa[1]	9.5 MPa[2]	20.3 MPa[2]
Deflection check	Less than Span/500	88.8 mm (18 mm)	17.7 mm[3] (12 mm)
Vibration serviceability	$f_1 > 5$ Hz	6.2 Hz	11.8 Hz

[1] : Based on maximum strength of 340 MPa.
[2] : Maximum principal stress among all components in FE model.
[3] : Refer to text for explanation of non-conformance.

Table 2
Input material properties of pGFRP – average from 10 tests (Thickness: 6 mm and 9 mm).

Property	Unit	6 mm	CoV (%)	9 mm
Longitudinal elastic modulus, E_L	GPa	23.0	5.2	24.6
Transverse elastic modulus, E_T	GPa	10.3	2.9	10.0
Major Poisson's ratio, ν_{LT}	–	0.30	–	0.31
Minor Poisson's ratio, ν_{TL}	–	0.15	–	0.14
In-plane shear modulus, G_{LT}	GPa	4.45	5.9	–

3.2. Bonding sequence

A two-part epoxy (R180 epoxy resin and H180 hardener supplied by Fibre Glass International) was mixed proportionally to adhesively-bond all pGFRP components. The lightweight nature of pGFRP components allows the MB to be constructed in an upside-down sequence – building the sandwich deck first then bonding the I-beams on top of the deck to form the underside of the MB. This construction sequence also complements various aspects of construction, such as the handling of epoxy, precision in aligning pGFRP components, and instrumentation (described in detail later).

A precise bonding procedure is adopted throughout construction of the MB to ensure quality of epoxy bonding. Prior to bonding operations, all bonding interfaces were roughened to improve the adherence of epoxy to pGFRP components. All bonding surfaces were vacuumed and cleaned using isopropanol to remove dust and improve adherence. Furthermore, all bonding operations were conducted on a temporary levelled super-flat construction platform, made from concrete formwork plywood, designed specifically for the construction of the MB. After each bonding operations, clamping pressure is applied onto the bonded surfaces – lead weights are used to add compression onto plane surfaces while G-clamps were applied onto vertical or underside bonding surfaces.

The bonding sequence of the MB is shown in Fig. 7(a – i). The lightweight of pGFRP components allows bonding procedures to be done with minimal use of heavy machinery and tools. The sandwich panel deck is made from four module segments (one shown in Fig. 7a) which are bonded together via connecting plates highlighted in Fig. 5a. This segmented bonding of modules improves time efficiency between bonding and the hardening period of different modules. The bonded modules are constructed without flat panels of the underside of the MB (Fig. 7b) to allow instrumentations of sensors within the deck (later described). Once the underside flat panels were bonded to form the completed sandwich deck, the I-beams and by T-sections were subsequently bonded onto the sandwich deck (underside of the MB). Wooden

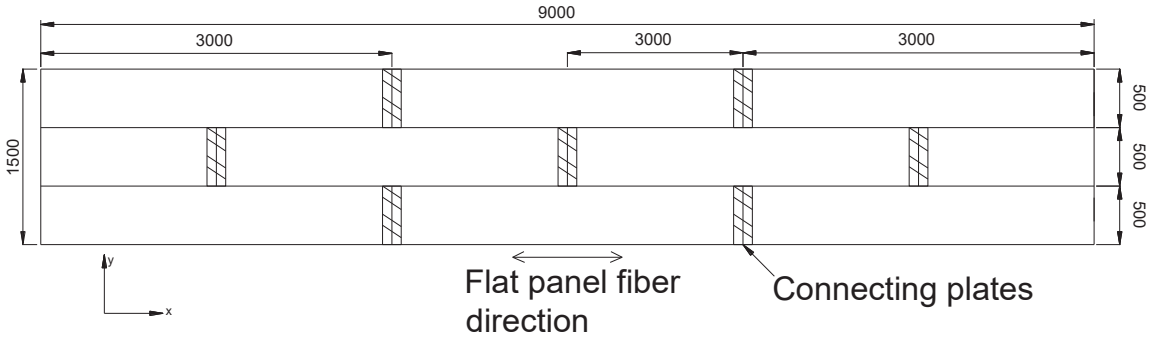

(a)

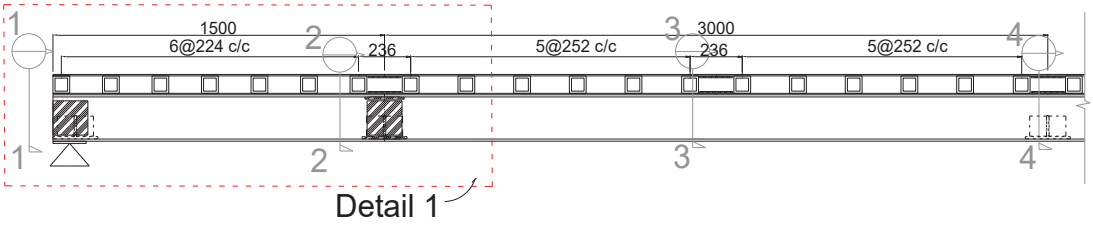

(b)

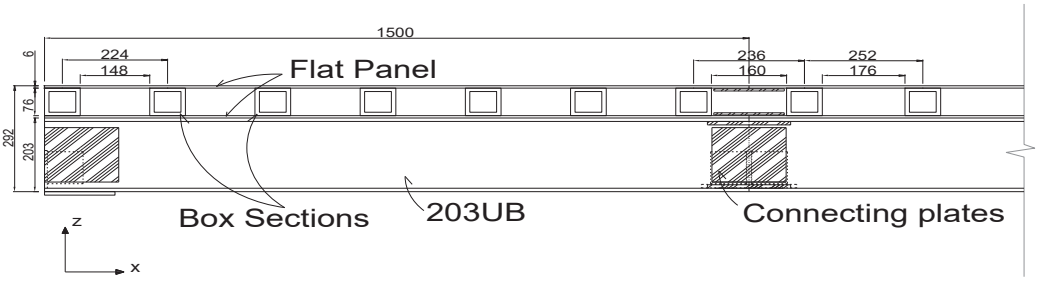

(c)

Fig. 5. Typical dimensions of the MB showing built-up of individual pGFRP components: a) plan view; b) elevation view of MB up to midspan (same disposal from both ends), and c) closeup of Detail 1 (units: mm).

spacers were used to help align the I-beams during bonding procedures. The completed MB, weighing about 900 kg, was then rotated using an overhead crane. Finally, the temporary construction platform was removed, and the MB was lifted to its final position.

3.3. Instrumentation

Instrumentation was installed in parallel with the construction process of the MB since there is easier access to regions such as within or underside of the beams and deck. A total of 70 strain gauges (FRA-10 supplied by TML, Japan) were installed along the MB. Each strain gauge has a gauge factor of 2.11 ± 1 %, and measures strains to a maximum of 5%. The strain gauges are installed in two configurations, namely as a single gauge or a strain rosette (Fig. 8b - c). The former measures strain in the strain gauge direction while the latter allow shear and principal strains to be determined. The strain gauges were positioned such that the strain distribution along the depth and width of the composite section can be captured. Gauges on the top surface were placed in a shallow groove about 1–2 mm depth, to minimize interference of the flat top surface. The cables of strain gauges that are mounted on the sandwich deck (top and bottom flat panel) were drawn from within the sandwich panels and in turn, directed out to the data acquisition point.

3.4. Manufacturing challenges and solution

The major challenge in the construction process was to control the high fluidity (runny) epoxy. Additionally, the control of bond thickness was important to manage due to the runny epoxy. Despite the control measures, excessive epoxy resulted on some bonding interfaces and insufficient epoxy on other surfaces; both of which could cause problems for performance.

Fig. 9 shows connections with excess epoxy, with a description following each image. The epoxy generally requires over 24 h for sufficient hardening at room temperature. In instances of poor epoxy

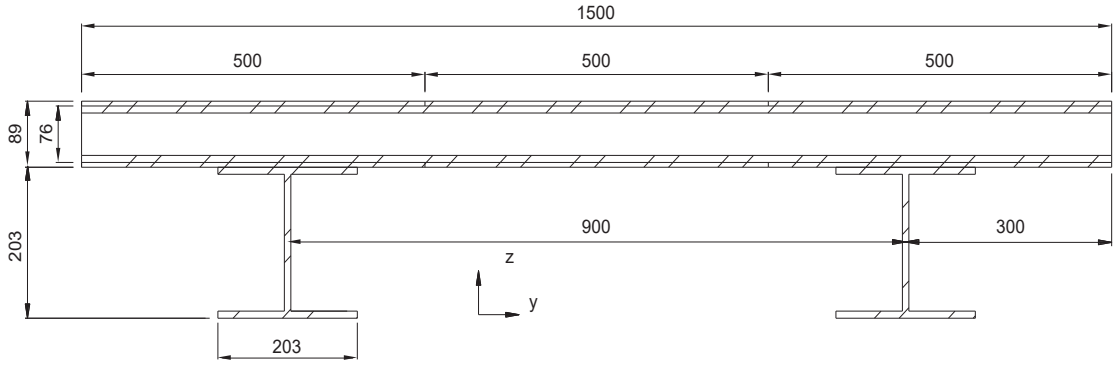

(a)

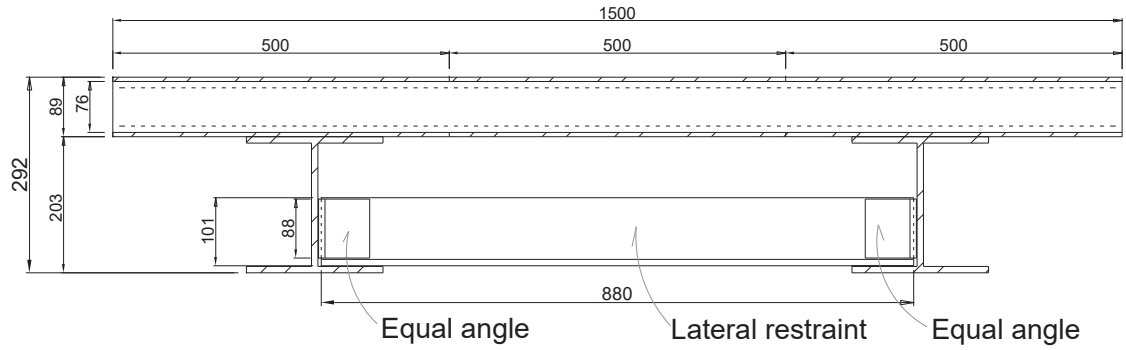

(b)

Fig. 6. Dimensions of cross-sections along the MB: (a) typical cross-section, and (b) cross-section with T-beams (units: mm).

control during this long hardening period, several connecting plates were covered in epoxy as shown in Fig. 9a. Additionally, strain gauges were to be installed on some of these connecting plates, compelling additional work in removing the hardened epoxy (Fig. 9b-c). Installation of the strain gauges on the deck was affected similarly, as seen in Fig. 9c. The control of excess epoxy was especially complicated for some non-trivial bonding interfaces (e.g. bonding of connecting plates onto underside of beam flange in Fig. 9d) and for bonding regions with multiple components (e.g. the section between T-section and beam flange in Fig. 9e). Furthermore, members at regions that lack visibility of bonding lines (e.g., attaching flat panel onto box profile core layer in Fig. 9f) were somewhat misaligned due to excess epoxy on some of their bonding surfaces.

The following aspects of the construction process were found to solve and alleviate the negative effects of runny epoxy in most bonding interfaces:

- The levelled construction platform helped eliminate any uneven surfaces of components (Fig. 10a), improving the control on epoxy on the bonding surfaces.
- Taping along the bonding region facilitates easy removal of excess (unhardened) epoxy (Fig. 10b).
- To ensure a uniform epoxy bond thickness, 5 mm-long wire spacers of 0.7 mm diameter were superglued at regular intervals along the bonding surfaces to ensure a uniform thickness of all bond lines (Fig. 10b). The spacers provide gaps in between bonding components, which also reduces undesirable epoxy seepage when the instance clamping pressures were applied onto bond interfaces.

With the experience gained and techniques developed, high quality repeatable bonds between the pGFRP components resulted in the majority of the bonding interfaces. Overall, the construction process of the MB demonstrated the potential of solely epoxy-bonding in modular construction of similar footbridges.

4. Static performance

4.1. Static loading tests

For static performance, the MB is tested under static loading test as shown in Fig. 11. The MB was loaded up to a uniformly distributed load level of 4.07 kN/m^2 (following the AASHTO guideline [15]). Three span configurations, namely an 8.785 m single-span (Test 1), a 6 m single-span (Test 2) and a 4.39 m two-span (Test 3), were tested. For Test 3, the loading was performed on one span to evaluate continuous-span behaviour of the MB. Fig. 12 shows the experimental setup for the static loading test. Vertical deflections were measured using Linear Voltage Displacement Transducers (LVDTs). Four C10 HBM load cells were placed at the support ends of the pGFRP I-beam girders. The load cells can measure static and dynamic forces up to 25 kN with accuracy class of 0.04% (i.e., maximum load cell deviation specified as percentage). For Test 3, two additional 50 kN load cells were used at the middle support.

4.2. Load-deflection responses

Fig. 13 shows the load–deflection responses (Test 1, 2, and 3). The

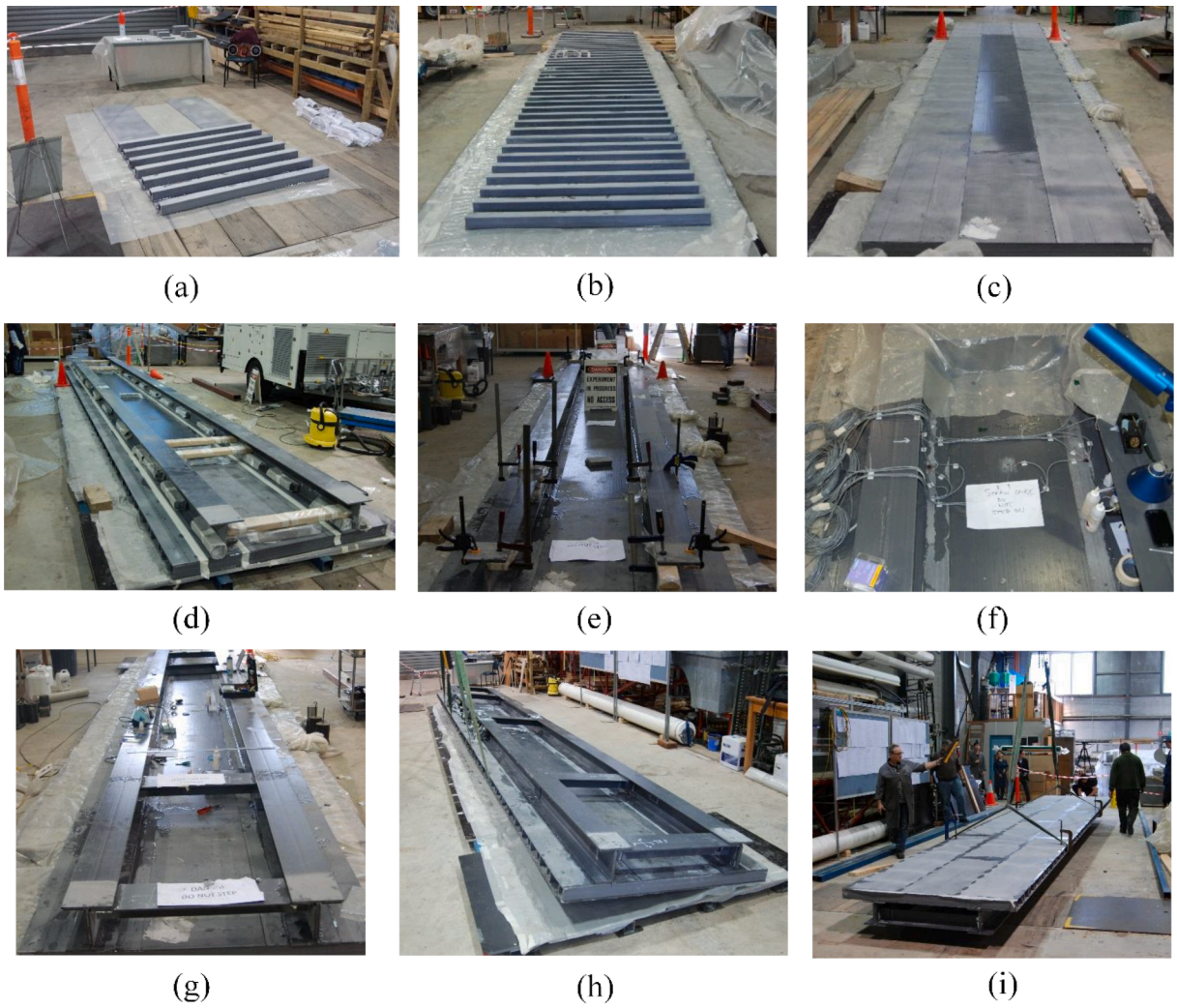

Fig. 7. Construction sequence: (a) fabrication of sandwich modules; (b) joining of modules; (c) bonding of flat panel layer; (d) bonding of I-beam girders; (e) installation of bond plates between I-beam sections (f) installation of under deck strain gauges; (g) attaching of the T-sections; (h) flipping of MB, and (i) lifting of MB to final position.

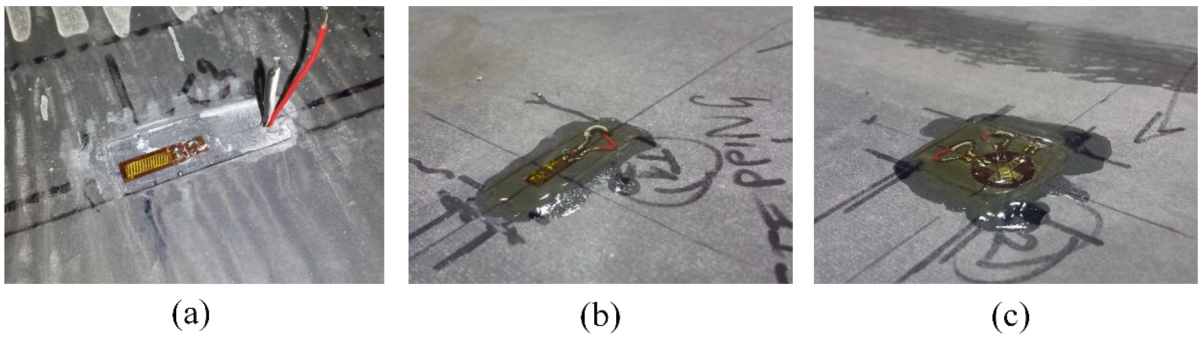

Fig. 8. Strain gauges: (a) showing recessed properties and through panel wiring, (b) single strain gauge sealed with clear epoxy coating, and (c) strain rosettes.

MB displayed linear-elastic load–deflection responses up to the maximum applied load (4.07 kPa). Table 3 presents the comparison of maximum midspan deflection between measurements and FE model. For Test 3, additional spring support configurations were incorporated in the FE model at locations correspond to the load cells at midspan. Apart from Test 3, the FE model predicted the maximum deflections of Test 1 and Test 2 with reasonable accuracy, as can be seen.

To evaluate the difference in deflections, the bending stiffness, *EI*, of the MB cross-section was calculated from the load–displacement curves using Euler-Bernoulli beam theory. The bending stiffness was found to be 6.61×10^{12} Nmm^2 for Test 1 and 6.02×10^{12} Nmm^2 for Test 2 (with a difference less than 10%). However, the bending stiffness for Test 3 was 2.58×10^{12} Nmm^2, which was about 60% lower than those calculated for Tests 1 and 2. This significant difference is due to the substantial shear deformations in the shorter 4.39 m span, which is not accounted for in Euler-Bernoulli beam theory.

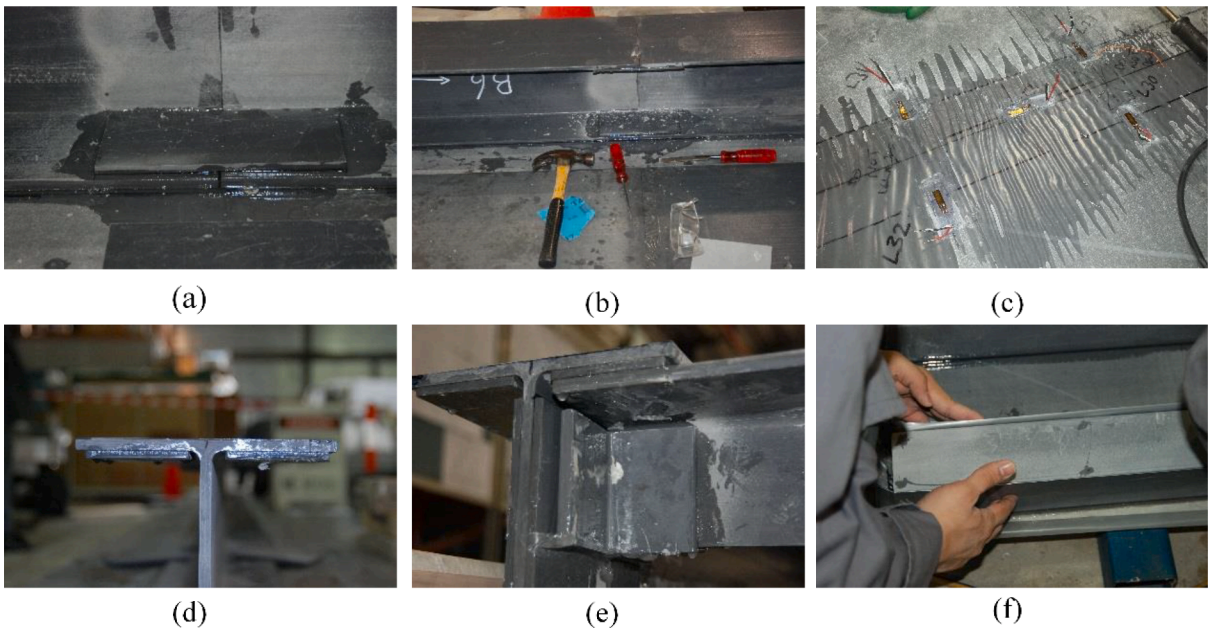

Fig. 9. Instances of difficult and/or inadequate control of running epoxy: (a) overflow of running epoxy, (b) removal of additional epoxy to access flange surface, (c) overflow of epoxy onto deck surface, (d) underside bonding of bond plates with beam flange, (e) multi-component bonding, and (f) misaligned box profiles.

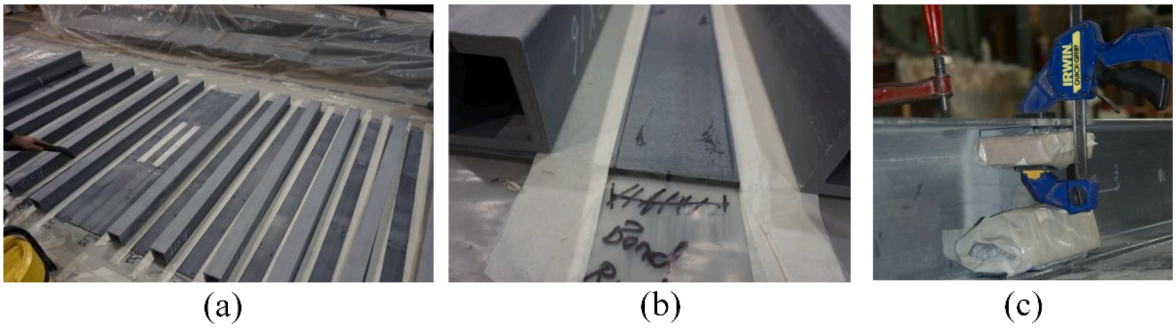

Fig. 10. Bond control operations: (a) cleaning and taping, (b) spacer wires along bond lines, and (c) clamping means through weights and G-clamps.

To account for shear stiffness, the bending stiffness is instead evaluated using Timoshenko beam theory [42] for Test 3. The MB in Test 3 can be considered as a single span propped cantilever continuous beam. The effective shear area is calculated using Bank's formula [43], assuming total shear area is equal to the two I-girders of the MB [41]. This results in a shear coefficient of 0.278. As a verification, Cowper's formula [44] for shear coefficient is used and obtained a shear coefficient of 0.281, which is relatively close to that from Bank's formula. With the shear contribution to total deflection, the revised bending stiffness, *EI*, for Test 3 becomes 5.5×10^{12} Nmm^2, which was only 9% less than that found using Euler-Bernoulli beam theory for Test 2. This observation is as expected: shear deformation is significant for the shortest span, contributing around 51% of the overall deflection. Therefore, Timoshenko beam theory should be considered for serviceability checks of lower span-to-depth ratio of the MB, which in fact is far higher for comparable footbridges of traditional materials (e.g., steel and concrete [45,46]).

4.3. Strain distributions

The strain distributions for sagging over the cross section were measured in each test and are shown in Fig. 14. According to Fig. 12, the measurement locations are at cross section CS4-4 for Test 1 and 2, and CS1-1 for Test 3. It is clear from Fig. 14 that the longitudinal strain distributions present a linear trend in two ranges: below 200 mm (from the lower flat panel to lower flange of I-beam), and above this (the sandwich deck). Further, there are compressive strains above the 200 mm depth (from the lower flat plate to upper flat plate), and tensile strains below this level. There is continuity in the strain profile at the interface between the sandwich deck and I-beam indicating that full composite action was provided by the adhesive bonding. This level of composite action (full across entire depth of MB) was not observed in previous small-scale testing [9] and its enhancement may be due to the higher web thickness of the footbridge sandwich deck, which used 9.5 mm-thick box-profiles compared to the 6 mm thickness used previously [9]. Overall, it is found that full composite action across the bridge deck is achieved by combining the use of epoxy bond and thicker box profiles.

5. Dynamic performance

5.1. Tests setup

The dynamic performance includes the evaluation of modal properties and vibration serviceability performance - particularly to evaluate the adopted 5 Hz rule. It should be noted that the experimental testing was conducted as parts of two larger research programmes – i.e., human-structure interactions and design rules for pGFRP footbridges. In turn, the full details of the experimental setups can be found in companion

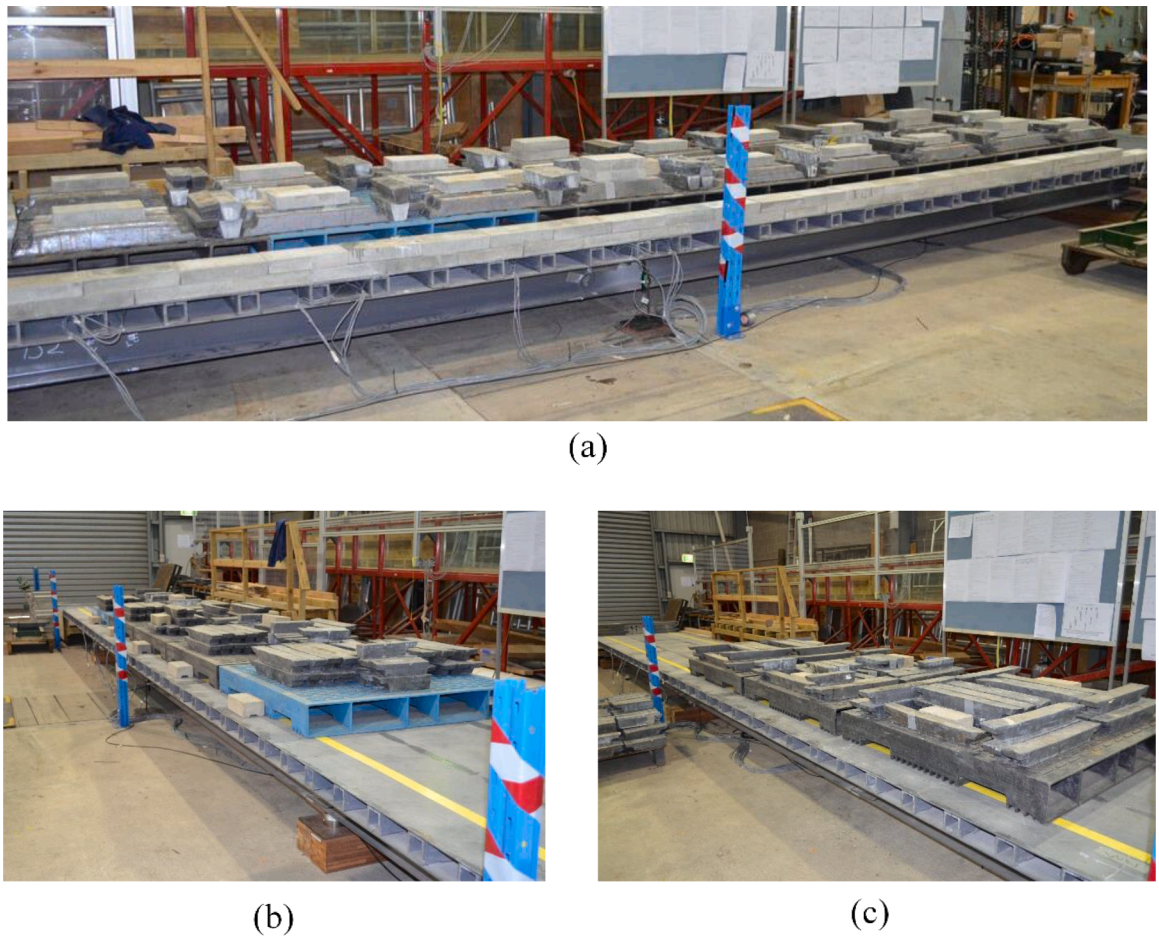

Fig. 11. Static Tests: (a) Test 1 – 9 m single-span, (b) Test 2 – 6 m single-span, and (c) Test 3 – 4.39 m two-span.

papers ([47,48]) and only a brief overview of each test's setup is given herein for brevity.

The experimental setup for dynamic performance testing is shown in Fig. 15. Experimental modal analysis (EMA) was performed to determine the modal properties of the MB for the 8.785 m span configuration (Test 1). The MB is excited using an electrodynamic shaker (denoted as shaker test). Vertical accelerations were measured using 10 piezoelectric accelerometers in a measurement grid as shown in Fig. 16a. The position of the shaker was placed offset the symmetric line of the MB, at quarter spans, to excite a range of bending and torsional modes.

As an additional verification, a separate hammer test is performed using three accelerometers as shown in Fig. 16b. The hammer strikes are roved across the three accelerometer positions during each measurement.

Following EMA, limited walking trials were performed to evaluate the vibration serviceability performance of the MB. Notably, vibration responses from walking trials allow for the evaluation of the design rules adopted in the MB (i.e., the 5 Hz rule). Three test subjects (TSs) participated in this walking trial, with properties summarized in Table 4. Five acceptable (in terms of realized pacing frequencies) walks were performed for each test subject at pacing frequencies (f_p) of 1.95 Hz, 1.8 Hz, and 2.1 Hz, intended to bracket the third harmonic excitation. Since the target resonant mode is Mode 1 (first bending), the acceleration responses were measured from two accelerometers placed on both sides at mid span of the MB – i.e., the anti-nodes of Mode 1.

5.2. Modal properties

Fig. 17 shows the mode shapes of the MB obtained from experimental modal analysis. For comparison, the predicted mode shapes from the FE model of the MB are presented in Fig. 18. The natural frequencies of the first six vibrational modes (f_1 to f_6) from the tests and the FE model are summarized in Table 5. The Modal Assurance Criterion (MAC) [49] – a correlation index between 0 and 1 - is calculated for the mode shapes between FE model and shaker test in Table 5. The MAC indicates good correlation for first three modes shapes (MAC values close to 1). The lower MAC for higher vibrational modes (fourth, fifth and sixth) is most likely due to the limited measurement points in EMA to capture the mode shapes. The modal damping for all vibrational modes is generally low (less than 1%), which is expected for pGFRP composites with inherent low material damping, and for a structure with no ancillary attachments. Indeed, the modal damping ratios are lower compared to other GFRP footbridges reported in the literature (between 2% and 5% [31,50–53]). This is almost certainly due to the simple geometry of the MB, having no complicated attachments such as handrails for example. Interestingly, the damping ratios are found to be amplitude dependent [54].

5.3. Vibration serviceability performance

The walking trials of the test subjects are simulated using a moving force (MF) model, based on common practice specified in [55]. For this study, Young's dynamic load factors (DLFs) [56] up to four harmonics are considered for the MF model. A typical one-dimensional (1-D) Euler-Bernoulli beam model of the MB is considered in the MF model simulations. Two bridge frequencies are considered for the 1-D model, namely from shaker test (5.86 Hz) – to account for potential mass loading – and from the hammer test (6.10 Hz). The damping ratio used

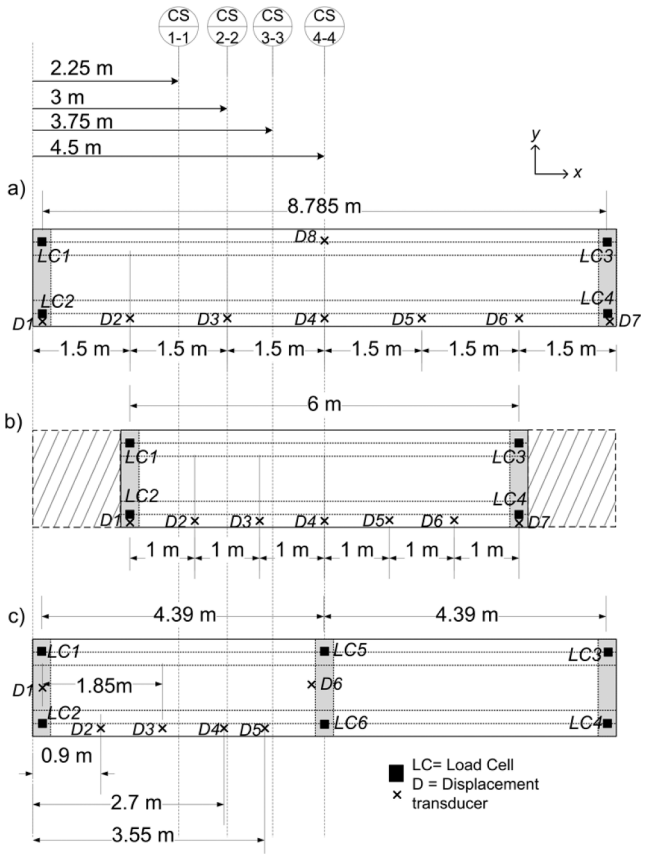

Fig. 12. Plan view showing cross-sections and positions of measurement locations for: (a) 8.785 m simply supported (Test 1); (b) 6 m simply supported (Test 2); (c) 4.39 m continuous two spans (Test 3). (after [41]).

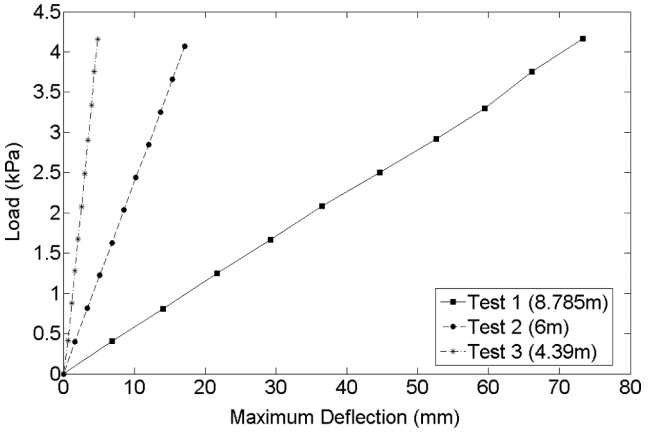

Fig. 13. Load vs maximum midspan deflections for Test 1, 2 and 3 of the static tests.

Table 3
Maximum midspan deflection of the MB between measurements and FE model.

Static tests	Measured (mm)	FE model(mm)	Error (%)
Test 1 (8.785 m)	77.7	88.8	12.5
Test 2 (6 m)	16.5	17.7	5.6
Test 3 (4.39 m)[1]	4.9	3.7	32.5

[1] : Readings of midspan deflection from a single span – 4.39 m.

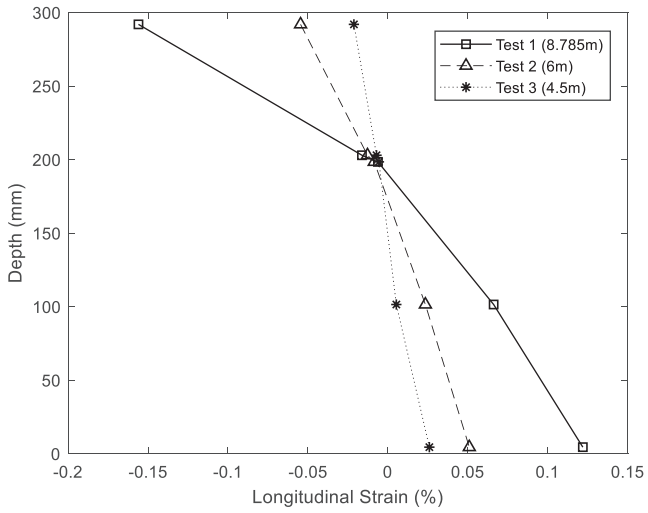

Fig. 14. Longitudinal strain distributions through specimen depth.

in the simulation is amplitude-dependent, which are obtained for each cycle of the accelerations from the free vibration portion of the acceleration responses.

Fig. 19 shows the vibration responses of the MB from the walking trials. The maximum mid-span accelerations are given in Table 6 alongside the results from the MF model. As can be seen, the MB attained high levels of accelerations from the third harmonic of walking frequencies even though the footbridge has a natural frequency of 6.1 Hz (i.e., it conforms to the 5 Hz rule). The measured responses can be compared with the limits in the Sétra guideline [57]. as shown in Table 7. It is clear from Fig. 19 that the acceleration responses from walking trials reaches the CL4 comfort level (unacceptable discomfort). Therefore, the traditional 5 Hz rule from AASHTO guideline [19] is not suited for the design of the MB, and so more generally it shows that current rules are not applicable for all GFRP footbridges.

Table 6 shows that the MB natural frequency (f_{b1}) of 5.86 Hz presents the resonant response of the MB (evident by the large responses of all TS). The predicted vibration responses were overestimated for TS1 and TS2 but underestimated for TS3, the test subject with the largest mass. The differences between measurements and simulations are presumably due to interactions in the human-structure dynamic system that are not captured by the relatively simple moving force model. It is apparent that the presence of test subject affects the dynamic response of the MB by way of contributing additional stiffness and damping [58], which consequently interacts with the dynamic properties of the MB. The study of this phenomenon is beyond the scope of this paper and has been covered elsewhere, see [59].

5.4. Discussions

Based on the results in Table 5, the uniformly lower natural frequencies from the shaker test infers the mass loading of the shaker. In other words, the shaker mass is significant to the mass of the bridge (about 5.6%). From the hammer test, the first natural frequency of the MB, f_1 is 6.17 Hz, which is closer to the natural frequency from the FE model (6.2 Hz) since the FE model does not consider the shaker mass. Nonetheless, the dynamic properties predicted from FE model are reasonable despite the lack of mass loading representation in the FE model.

Close inspection on the measured mode shapes in Fig. 17 reveals a slight asymmetric modal behaviour in the first and third mode. Interestingly this phenomenon is still observed even after repeated tests for verification in which the shaker test was repeated by moving the shaker [60]. Since the shaker does not explicitly contribute stiffness to the overall stiffness of the system, the asymmetric modal behaviour may

Fig. 15. Experimental modal analysis setup with electrodynamic shaker and accelerometers.

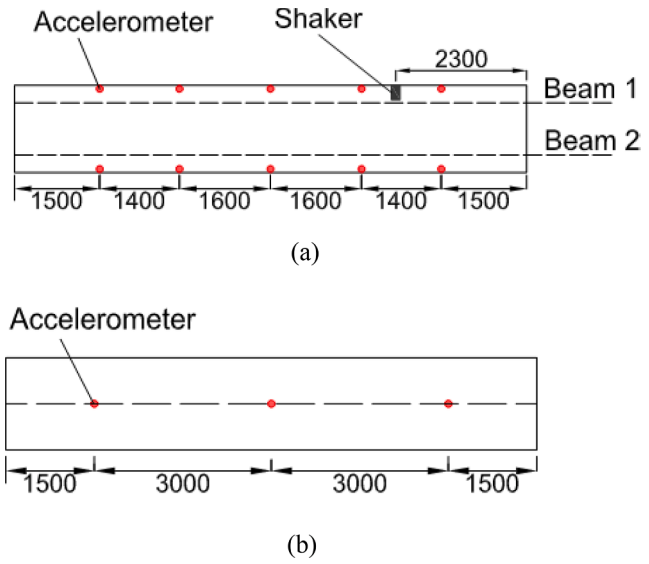

Fig. 16. Measurement grid for: (a) shaker tests, and (b) impact hammer tests.

Table 4
Properties of participants of walking trials.

Test Subject	Weight (N)	Height (cm)
TS1	624	170
TS2	706	178
TS3	1060	183

stem from the shaker mass balancing out some anomaly in longitudinal stiffness. Possible sources leading to deviation of longitudinal stiffness can be due to: (i) geometric deviations introduced during construction, or (ii) material properties deviations (further assessed in [60]). Detailed study on this interesting phenomenon is beyond the scope of this paper and has been subjected in the research presented in [61].

The mass loading of the electrodynamic shaker in the vibrating system of the MB as seen in Section 4.3 infer a similar mass loading phenomenon of test subjects during walking trials. Consequently, accurate simulation of walking trials of test subjects (TS1 to TS3) requires the consideration of human-structure system in the MB. This means that the use of an interactive human force model to account for structural interactions of test subjects should give more faithful results – this was investigated in [47]. For this work, the simple moving force model is considered to evaluate the walking forces of the test subjects on the basis of common practice (current design guidelines [62]).

6. Summary and conclusions

This paper summarizes the relevant aspects of the design, construction, and performance testing of the Monash pGFRP footbridge (MB). The MB has a length and width of 9 m and 1.5 m respectively. The MB presents a novel orthotropic pGFRP sandwich deck configuration which comprised of standard pGFRP profiles. The orthotropic pGFRP sandwich panel adopts bidirectional fibre orientation which optimizes strength capacities in both orthogonal directions. The entire MB is adhesively bonded throughout, i.e., no mechanical bolts were used.

The MB was purpose-built for a variety of research goals. The design process of the MB was facilitated using a numerical FE model. The MB adopted ASHTO's Guide Specifications for Design of FRP Pedestrian Bridges for its limit state design, namely allowable stress design and deflection checks. A compromise in deflection requirement was reached in the final design of the MB (full span) in order to achieve a desired dynamic behaviour of the MB for research - having a first natural frequency greater than 5 Hz yet lying within harmonic ranges of human walking forces.

The lightweight and modular concept of the MB render construction possible with minimal use of heavy machinery or tools. Owing to its small mass, the MB was constructed upside down and flipped to its final disposition after completion. The design of the MB demonstrates the potential of using standard pGFRP profiles in modular construction. The major issue during construction relates to the control of runny epoxy in

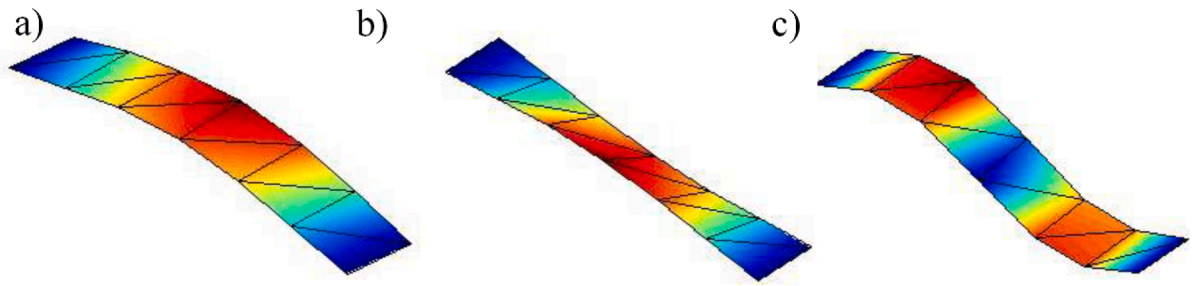

Fig. 17. First three modes of vibration obtained from shaker test: (a) $f_1 = 5.86$ Hz, (b) $f_2 = 10.02$, (c) $f_3 = 18.14$ Hz.

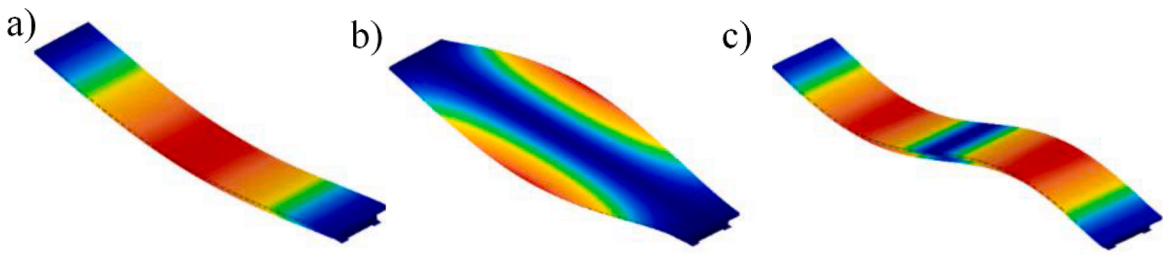

Fig. 18. First three modes of vibration from FE model: (a) $f_1 = 5.95$ Hz; (b) $f_2 = 9.62$ Hz; (c) $f_3 = 20.27$ Hz.

Table 5
Comparison between natural frequencies from experiment and FE model. Damping ratios are from shaker test.

Mode	Natural frequency (Hz) Shaker test	Hammer test	FE model	Diff (%)[1]	Damping, ξ (%)	MAC[2]
1	5.86	6.17	5.95	1.5	0.59	0.98
2	10.02	–	9.62	4.0	0.96	0.97
3	18.14	19.60	20.27	11.7	0.61	0.98
4	20.60	–	23.87	15.9	1.65	0.64
5	25.60	–	28.85	12.7	1.33	0.66
6	37.54	38.30	39.52	5.3	0.92	0.85

[1] : Natural frequency differences between shaker and hammer tests.
[2] : Modal assurance criterion.

bonding procedures and the adopted solutions are discussed. Overall, the construction process of the MB demonstrates the potential of epoxy-bonding for modular construction of similar footbridges.

The static performance of the MB includes the evaluation of deflection and strain distributions under design service load. Static tests were performed by loading the MB up to design service load (4.07 kN/m^2) for multitude of span configurations. The results showed that the deflection response is linear for various span configurations of the MB. Results from FE prediction are in good agreement with the measured deflections except for the shorter span configuration (4.39 m double span). Shear deformation was found to be significant towards on the bending stiffness for shorter spans, accounting for 51% of the overall deflection. In contrast, it is much smaller for the longer span tests (8.785 m single span). Consequently, this showed that shear deformations in deflection serviceability checks is more significant for pGFRP structures than for structures of traditional materials. Finally, the results from the measured

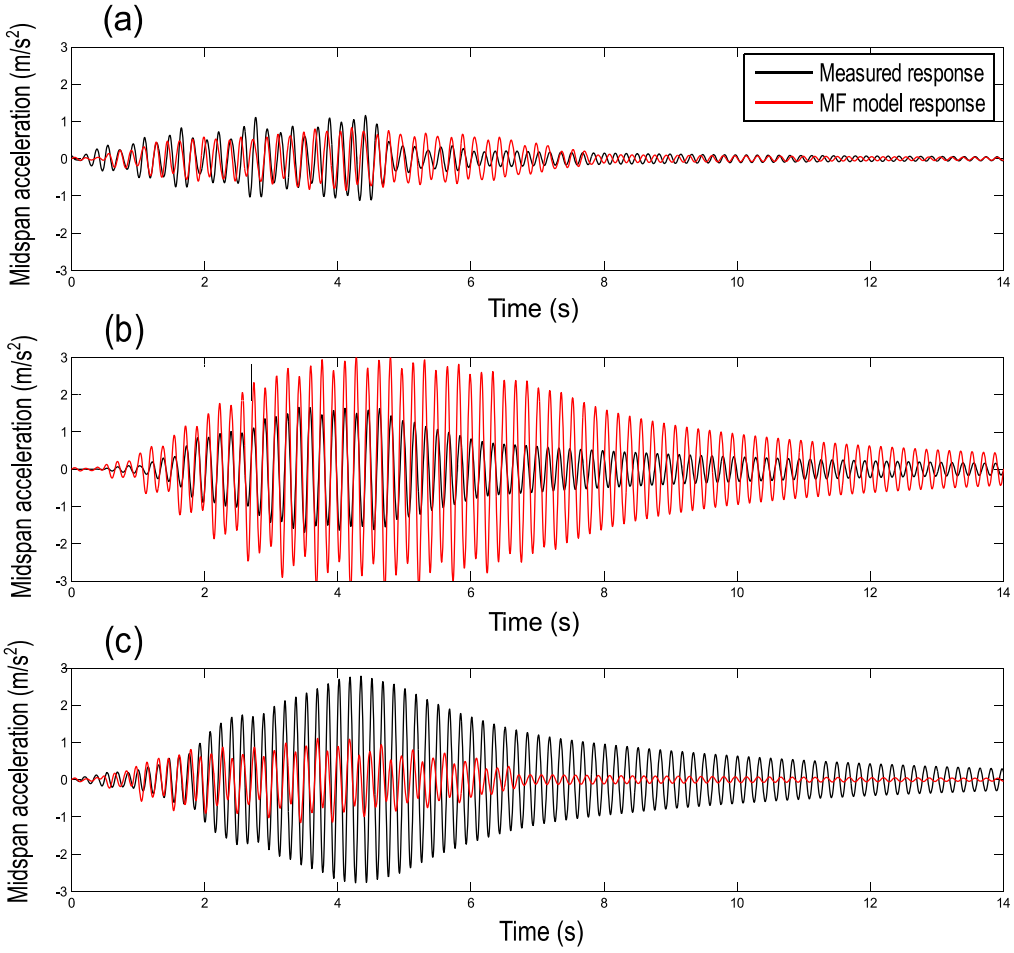

Fig. 19. Measured and simulated vibration response for TS3 and pacing frequency of: (a) 1.8 Hz (b) 1.95 Hz (c) 2.1 Hz. (after [48]).

Table 6
Maximum mid-span accelerations from measurements and numerical moving force model. Units in m/s^2.

TS	f_p (Hz)								
	1.80			1.95			2.10		
	Measured	MF Model f_{b1} (Hz)		Measured	MF Model f_{b1} (Hz)		Measured	MF Model f_{b1} (Hz)	
		5.86	6.10		5.86	6.10		5.86	6.10
1	0.38	0.50	0.35	0.74	2.45	1.06	0.66	0.68	1.36
2	0.32	0.57	0.40	0.61	2.64	1.19	0.67	0.77	1.52
3	1.16	0.85	0.60	2.26	3.27	1.71	2.86	1.16	2.17

Table 7
Comfort levels from Sétra guidelines [57].

Comfort Level	Degree of comfort	Vertical acceleration limits (m/s^2)
CL 1	Maximum	< 0.5
CL 2	Medium	0.5 – 1.0
CL 3	Minimum	1.0 – 2.5
CL 4	Unacceptable	> 2.5

strain distributions showed that full-composite action is achieved by adhesive bonding of connections.

Dynamic performance of the MB includes the evaluation of modal properties and vibration response under human walking. Experimental modal analyses were performed to determine the modal properties of the MB. The FE model was able to predict the mode shapes and natural frequencies of the MB with reasonable accuracy. The first natural frequency of the footbridge conforms to the 5 Hz rule and yet lies in the third harmonic range of human walking frequency. The damping ratios for first six vibrational modes were estimated between 0.6% and 1.65%, which are relatively lower than comparable GFRP footbridges (between 2% and 5%). This is most likely due to the simple geometry of the MB, having no complicated attachments such as handrails for example. Comparison of mode shapes between FE model and measurements reveals an asymmetric behaviour in the measured bending modes (Mode 1 and Mode 3). Further shaker tests verified that the mass of the shaker is somewhat balancing out anomalies in structural stiffness. Finally, walking trials were performed and the results of acceleration responses showed that the MB attained high accelerations despite meeting the 5 Hz design rule. The results also infer the use of interactive human models for better representation of vibration responses from numerical models.

The experience gained from the design and construction of the MB indicates the many significant advantages of pGFRP in footbridge applications. The light weight, modular nature, and constructability makes it easy to transport and particularly well-suited to common short footbridge spans. Furthermore, the design process of the MB showed that current numerical and analytical methods can be readily applied for design of such structures, but with some refinements required. Indeed, the performance of the MB shows that the current rules for GFRP footbridges do not apply to all GFRP bridges; in particular, the MB exhibits insufficient vibration serviceability performance despite conforming to current design rules for vibration. Consequently, there is a need for further development of design guidelines for pGFRP footbridges, especially for vibration serviceability, to fully exploit the merits of pGFRP in bridge construction.

Declaration of Competing Interest

The authors declare that they have no known competing financial interests or personal relationships that could have appeared to influence the work reported in this paper.

Acknowledgement

This work is supported by the Monash University Faculty of Engineering Seed Funding Scheme. The authors would like to thank all laboratory staff of the Monash University Structural Laboratory for their role and contribution towards the construction and testing works of the MB. The authors also acknowledge student contributions of Julio Bintoro, Gustavo Carvalho, Chris Keys, and Henrique De Salles towards the construction and testing of the MB.

References

[1] A. Żyjewski, J. Chróścielewski, and Ł. Pyrzowski, "The use of fibre-reinforced polymers (FRP) in bridges as a favourable solution for the environment," *E3S Web Conf.*, vol. 17, p. 00102 %U 10.1051/e3sconf/20171700102, 2017.
[2] Karbhari V, Seible F. Fiber Reinforced Composites – Advanced Materials for the Renewal of Civil Infrastructure. Appl Compos Mater 05/01 2000,;7:95–124. https://doi.org/10.1023/A:1008915706226.
[3] T. Keller, "Use fo Fibre Reinforced Polymers in Bridge Construction " in *(SED 7) IABSE*, Zurich, 2003.
[4] Birman V, Kardomateas GA. Review of current trends in research and applications of sandwich structures. Compos B Eng 2018;142:221–40.
[5] Manalo A, Aravinthan T, Fam A, Benmokrane B. State-of-the-Art Review on FRP Sandwich Systems for Lightweight Civil Infrastructure. J Compos Constr 2017;21 (1):1–16.
[6] Satasivam S. Modular FRP sandwich structures for building floor construction. Melbourne: Monash University; 2017.
[7] Hollaway LC. A review of the present and future utilisation of FRP composites in their civil infrastructure with reference to their important in-service properties. Constr Build Mater 2010;24:2419–45.
[8] Satasivam S, Bai Y. Mechanical Performance of bolted modular GFRP composite sandwich structure using standard and blind bolts. Compos Struct 2014;117:59–70.
[9] Satasivam S, Bai Y, Zhao XL. Adhesively bonded modular GFRP web-flange sandwich for building floor construction. Compos Struct 2014;111:381–92.
[10] Satasivam S, Bai Y, Yang Y, Zhu L, Zhao XL. Mechanical performance of two-way modular FRP sandwich panel. Compos Struct 2018;184:904–16.
[11] Satasivam S, Yu B. Mechanical performance of modular FRP-steel composite beams for building construction. Mater Struct 2016;49:4113–29.
[12] Siwowski T, Kaleta D, Rajchel M. Structural behaviour of an all-composite road bridge. Compos Struct 2018/05/15/ 2018,;192:555–67. https://doi.org/10.1016/j.compstruct.2018.03.042.
[13] L. Ye and P. Feng, "Applications and development of fiber-reinforced polymer in engineering structures," *Tumu Gongcheng Xuebao/China Civil Engineering Journal*, Review vol. 39, no. 3, pp. 24-36, 2006. [Online]. Available: https://www.scopus.com/inward/record.uri?eid=2-s2.0-33748713098&partnerID=40&md5=391a336b230fc9f8eb4fbfa33d14ec25.
[14] J. D. Plunkett, "Fiber-reinforced polymer honeycomb short span bridge for rapid installation," IDEA Project final report, Contract NCHRO-96-ID030, 1996.
[15] J. Cadei and T. Stratford, "The design, construction and in-service performance of the all-composite Aberfeldy footbridge," *Advanced Polymer Composites for Structural Applications in Construction*, vol. ed. / Ajit Shenoi; Stuart Moy; Len Holloway. ICE Publishing, , pp. 445-453, 2002.
[16] Siwowski T, Kulpa M, Rajchel M, Poneta P. Design, manufacturing and structural testing of all-composite FRP bridge girder. Compos Struct 2018/12/15/ 2018,;206:814–27. https://doi.org/10.1016/j.compstruct.2018.08.048.
[17] Bank LC. Composites for construction: structural design with FRP materials. John Wiley & Sons; 2006.
[18] Mottram J. FRP Bridges - Guidance for Designers, (C779. London: CIRIA; 2019. p. 2019.
[19] AASHTO, "Guide Specification for design of FRP pedestrian bridges (1st ed.) ", ed: American Association of State Highway and Transportation Officials (AASHTO), 2008.
[20] H. England, "Design of fibre reinforced polymer bridges and highway structures," CD 368, 2020.
[21] Górski P, Tatara M, Stankiewicz B. Vibration serviceability of all-GFRP cable-stayed footbridge under various service excitations. Measurement 2021/10/01/ 2021,;183:109822. https://doi.org/10.1016/j.measurement.2021.109822.
[22] Wei X, Russell J, Živanović S, Toby Mottram J. Measured dynamic properties for FRP footbridges and their critical comparison against structures made of conventional construction materials. Compos Struct 2019/09/01/ 2019,;223:110956. https://doi.org/10.1016/j.compstruct.2019.110956.
[23] Zivanovic S, Feltrin G, Mottram JT, Brownjohn JMW. "Vibration Performance of Bridges Made of Fibre Reinforced Polymer," in *IMAC- XXXII*. USA: Orlando; 2014.

[24] Ji HS, Son BJ, Ma Z. Evaluation of composite sandwich bridge decks with hybrid FRP-steel core. ASCE J Bridge Eng 2009;14(1):36–44.
[25] Braestrup MW. Footbridge constructed from glass fibre-reinforced profiles. Struct Eng Int 1999;9(4):256–8.
[26] Fu C, AlAyed H, Robert J. Field performance of the fiber-reinforced polymer deck of a truss bridge. J Perform Constr Facil 2007;21(1):53–60.
[27] Smits J. Fiber-Reinforced Polymer Birdge Design in the Netherlands: Architectural Challenges towards Innovative, Sustainable and Durable Bridges. Engineering 2016;2:518–27.
[28] Russell JM, Wei X, Živanović S, Kruger C. Vibration serviceability of a GFRP railway crossing due to pedestrians and train excitation. Eng Struct 2020/09/15/ 2020,;219:110756. https://doi.org/10.1016/j.engstruct.2020.110756.
[29] Smits J. Fiber-Reinforced Polymer Bridge Design in the Netherlands: Architectural Challenges toward Innovative, Sustainable, and Durable Bridges. Engineering 2016/12/01/ 2016,;2(4):518–27. https://doi.org/10.1016/J.ENG.2016.04.004.
[30] Wan B. 1 - Using fiber-reinforced polymer (FRP) composites in bridge construction and monitoring their performance: an overview. In: Kim YJ, editor. Advanced Composites in Bridge Construction and Repair. Woodhead Publishing; 2014. p. 3–29.
[31] Gonilha JA, Correia JR, Branco FA, Caetano E, Cunha A. Modal identification of a GFRP-concrete hybrid footbridge prototype: Experimental tests and analytical and numerical simulations. Compos Struct 2013;106:724–33.
[32] R. L. Pimentel, P. Waldron , and W. J. Harvey, "Assessment of the dynamic behaviour of Aberfeldy GFRP plastic cable-stayed footbridge," ed. London: in Seminar on Analysis and Testing of Bridges, Institution of Structural Engineers, 1995, pp. 38-40.
[33] S. Živanović, J. M. Russell, and V. Racic, "Vibration Performance of a Lightweight FRP Footbridge Under Human Dynamic Excitation," in *Dynamics of Civil Structures, Volume 2*, Cham, S. Pakzad, Ed., 2020// 2020: Springer International Publishing, pp. 111-114.
[34] H. Dang and S. Živanović, "Influence of Low-Frequency VerticalVibration on Walking Locomotion," pp. 1-12, 2015.
[35] Živanović S, Pavic A, Reynolds P. Vibration Serviceability of footbridges under human-induced excitation: A literature review. Sound Vib 2005;279:1–74.
[36] Zhang SH, Caprani CC, Heidarpour A. Influence of Fibre Orientation on Pultruded GFRP Material Properties. Compos Struct 2018;204(15):368–77.
[37] ASTM, "D3039. Standard tst method for tensile properties of polymer matrix composite materials.," 2000.
[38] T.-T. Nguyen, T.-M. Chan, and J. T. Mottram, "Reliable in-plane shear modulus for pultruded-fibre-reinforced polymer sections," *Proceedings of the Institution of Civil Engineers - Structures and Buildings,* vol. 171, no. 11, pp. 818-829, 2018, 10.1680/jstbu.16.00194.
[39] "LUSAS User Manual v15-2.0," ed.
[40] M. Evernden and J. T. Mottram, "A case for houses to be constructed of fibre reinforced polymer components," *Proceedings of the ICE - Construction Materials,* vol. 165, pp. 3-13, 2012.
[41] Satasivam S, Caprani CC, Bai Y. "Static performance of an all-composite modular compostite beam under positive and negative bending scenarios," in *8th International conference on Fibre-Reinforced Polymer (FRP) Composites in Civil Engineering (CICE)*. Hong Kong: China; 2016.
[42] Timoshenko S, Goodier JN. Theory of Elasticity. 3rd ed. McGraw-Hill; 1969.
[43] Bank LC. Shear coefficients for thin-walled composite beams. Compos Struct 1987/01/01/ 1987,;8(1):47–61. https://doi.org/10.1016/0263-8223(87)90015-8.
[44] Cowper G. The Shear Coefficient in Timoshenko's Beam Theory. J Appl Mech 1966;33:335–40.
[45] Chen Y, Dong J, Xu T, Xiao Y, Jiang R, Nie X. The shear-lag effect of composite box girder bridges with corrugated steel webs and trusses. Eng Struct 2019/02/15/ 2019,;181:617–28. https://doi.org/10.1016/j.engstruct.2018.12.048.
[46] Ji WL, S. z.,. Vertical Deflection of Simply Supported Box Beam with Corrugated Steel Webs Including Effects of Shear Lag and Shear Deformation. Appl Mech Mater 2012;204–208:1012–6. https://doi.org/10.4028/www.scientific.net/amm.204-208.1012.
[47] Ahmadi E, Caprani CC, Živanović S, Heirdapour A. Vertical ground reaction forces on rigid and vibrating surfaces for vibration serviceability assessment of structures. Eng Struct 2018:723–38.
[48] Ngan JW, Caprani C, Bai Y. Dynamic Performance Assessment of a Novel Pultruded Fibre Reinforced Polymer Footbridge. in *Australasian Conference on the Mechanics of Structures and Materials ACMSM*. 2016.
[49] Allemang RJ. The Modal Assurance Criterion (MAC): Twenty years of use and abuse. J Sound Vib 2003;37(8):14–23.
[50] Aluri S, Jinka C, Gangarao HV. Dynamic response of three fiber reinforced polymer composite bridges. J Bridg Eng 2005;10(6):722–30.
[51] R. A. Votsis, T. J. Stratford, and M. K. Chryssanthopoulos, "Dynamic assessment of a FRP suspension footbridge," *ACIC- 09: Adv. Compos. Constr.*, 2009.
[52] Bai Y, Keller T. Modal parameter identification for a GFRP pedestrian bridge. Compos Struct 2008/01/01/ 2008,;82(1):90–100. https://doi.org/10.1016/j.compstruct.2006.12.008.
[53] Burgueño R, Karbhari VM, Seible F, Kolozs RT. Experimental dynamic characterization of an FRP composite bridge superstructure assembly. Compos Struct 2001/12/01/ 2001,;54(4):427–44. https://doi.org/10.1016/S0263-8223(01)00115-5.
[54] Ahmadi E, Caprani C, Živanović S, Evans N, Heidarpour A. A framework for quantification of human-structure interaction in vertical direction. J Sound Vib 2018/10/13/ 2018,;432:351–72. https://doi.org/10.1016/j.jsv.2018.06.054.
[55] Caprani C, Ahmadi E. Formulation of human-structure interation system models for vertical vibration. J Sound Vib 2016;377:346–67.
[56] P. Young, "Improved floor vibration prediction methodologies," ed: ARUP vibration seminar 2001.
[57] Setra, "Footbridges: Assessment of vibration behaviour of footbridges under pedestrian loading," ed. Paris: Technical guide, Service d'Etudes Techniques des Routes et Autoroutes, 2006.
[58] Z. Ibrahim, "The Effects of Crowd Dynamic Characteristics of Stadia Structure," PhD Thesis, The University of Sheffield, 2006.
[59] E. Ahmadi, "Human-structure interaction: experimentation and modelling for vertical vibration," PhD Thesis, Monash University, 2018.
[60] Ngan JW, Caprani C, Bai Y. "Model Updating of a GFRP footbridge using Tchebichef Moment Descriptors," in *9th International Conference on Bridge Maintenance*. Melbourne: Safety and Management; 2018.
[61] Ngan JW, Caprani C, Bai Y. Full-field Finite Element Model Updating using Zernike Moment descriptors for Structures Exhibiting Localized Mode Shapes. Mech Syst Sig Process 2019;121(16):373–88.
[62] P. Archbold, J. Keogh, C. C. Caprani, and P. Fanning "A parametric study of pedestrian vertical force models for dynamic analysis of footbridges," in *Proceedings of the EVACES - Experimental Vibration Analysis for Civil Engineering Structures*, 2011, pp. 35-44.